Geochemical modeling of acid-basic magma interaction in the Sardinia-Corsica Batholith: the case study of sarrabus, southeastern

ELSEVIER

Lithos 46 (1999) 553–571

LITHOS

Geochemical modeling of acid–basic magma interaction in the Sardinia–Corsica Batholith: the case study of Sarrabus, southeastern Sardinia, Italy

Giampiero Poli [a,*], Simone Tommasini [a,b]

[a] *Dipartimento di Scienze della Terra, Perugia, Italy*
[b] *Dipartimento di Scienza del Suolo e Nutrizione della Pianta, Firenze, Italy*

Received 5 January 1998; accepted 1 June 1998

Abstract

The Hercynian intrusive rocks outcropping in the Sarrabus area, southeastern Sardinia, Italy, consist of microgranular mafic enclave (MME)-bearing granites (> 95%) associated with coeval stratified gabbroic complexes and basic septa (BS) (< 5%). The coexistence of partially molten magmas of contrasting composition offers the opportunity to study interaction processes in intrusive environments and the geochemical characteristics of hybrid products. In this paper we present a petrogenetic model for the differentiation of basic magmas injected into coeval, partially molten, granite magmas, on the basis of field, petrographic and geochemical data. Samples from the stratified basic complex of Capo Carbonara (CCB) and BS were grouped into outer and inner facies based upon the sampling sites close to, or far away (a few meters) the host granite contact. MME were grouped according to their composition: gabbro-diorites and tonalites. The inner facies of the basic complex and BS represent cumulus of amphibole + clinopyroxene + plagioclase with trapped intercumulus liquid. The calculated chemical composition of the parental magma is well within those calculated for the Hercynian basic magmas of the Sardinia–Corsica Batholith. The geochemical features of the MME and the outer facies of the basic complex and BS establish an origin by mixing/mingling mechanisms controlled by fractional crystallisation and contamination (CFC) of the parental magma of the inner gabbroic facies. Additional refinements of the model, addressed in this paper, establish the occurrence of a filter pressing process operating during the CFC evolution of the basic magma injected into the acid magma.

Keywords: Sardinia; Granitoid; Contamination; Magma mixing; Magma mingling; Fractional crystallisation

1. Introduction

Acid–basic magma interaction plays a key role in granite petrogenesis where mantle-derived melts are injected into anatectic crustal levels (Vernon, 1984; Didier and Barbarin, 1991a, for a review). The dynamics and thermodynamics of interaction processes, in their general terms, are fairly well constrained (e.g., Frost and Lindsay, 1988; Campbell and Turner, 1989). On the other hand, the use of geochemical tracers as a robust tool to fingerprint the details of the processes occurring when basic magmas interact with acid magmas, are poorly explored.

* Corresponding author. E-mail: polig@egeo.unipg.it

0024-4937/99/$ - see front matter
PII: S0024-4937(98)00082-6

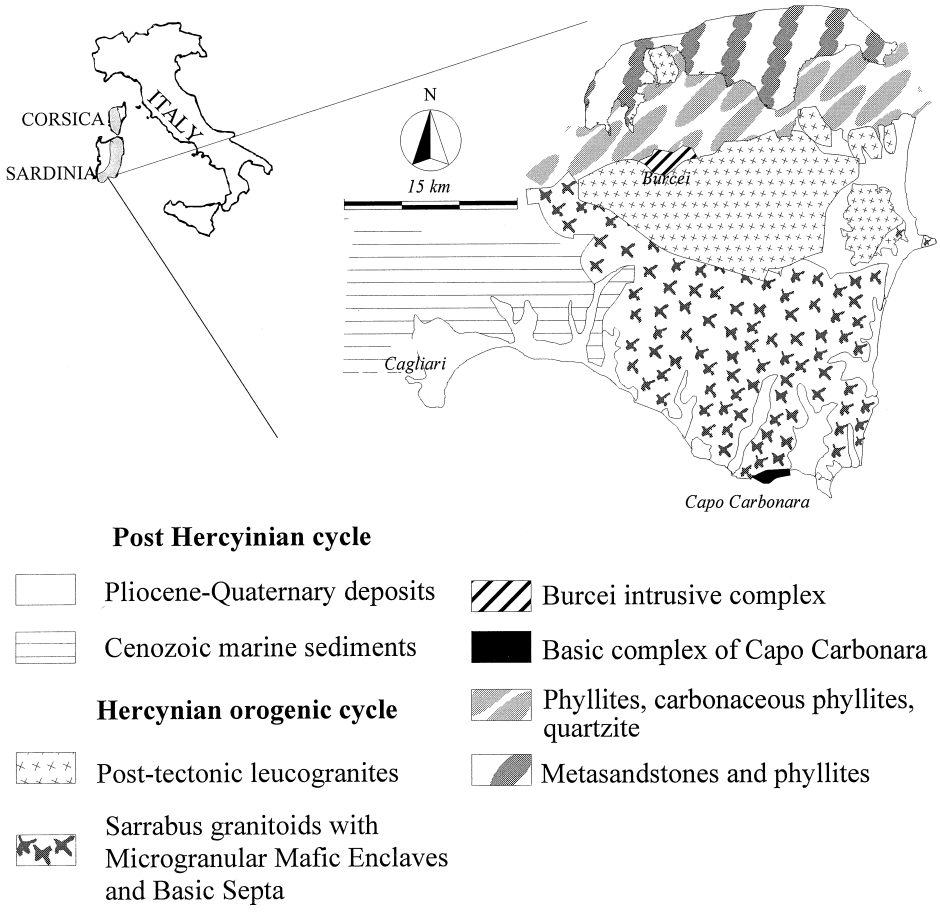

Fig. 1. Geologic sketch map of the Sarrabus area, southeastern Sardinia.

The Hercynian Sardinia–Corsica Batholith offers an excellent field laboratory to study interaction processes between magmas of contrasting composition. The Batholith was formed as a results of continental collision during the Hercynian orogeny in Southern Europe (e.g., Carmignani et al., 1992), and is largely composed of crust-derived granites and subordinate mantle-derived gabbros (Bralia et al., 1981; Cocherie, 1984; Poli et al., 1989; Tommasini, 1993; Cocherie et al., 1994). The interaction between crust- and mantle-derived magmas resulted in a wide variety of hybrid rocks ranging from homogeneous, completely blended tonalites, to heterogeneous, mechanically mixed, mafic enclave-bearing granites (Poli et al., 1989; Rossi and Cocherie, 1991; Zorpi et al., 1991; Tommasini, 1993). In this paper, we try to unravel the geochemical details of magma interaction in the southernmost sector of the Batholith (Fig. 1), where, in a relatively limited area (< 40 km^2), is possible to encounter most of the interaction-related products, from gabbroic complexes and BS to MME widely dispersed within the host granite.

2. Geology, petrography and mineral chemistry

The principal intrusive bodies in this sector of the Sardinia–Corsica Batholith (Fig. 1) are coalescent granite plutons (GP). Microgranular mafic enclaves (MME), as defined by Didier and Barbarin (1991b), form up to 3–5% of the total outcrop surface and commonly have ellipsoidal shapes, with maximum

dimensions up to 200×30 cm^2, suggesting a plastic rheology (i.e., a molten state) during enclosure in the host granite magma. Basic complexes ($< 5\%$), can occur as either discrete, sill-like body (a few meters wide and several tens of meters long), or stratified complexes with aspect ratio close to unity (generally some hundreds of meters in size). The former, hereafter defined as basic septa (BS, Poli et al., 1996), exhibit mechanical interaction phenomena along the contacts with the host granite, such as, for example, the presence of both interdigitation and xenocrysts/fragments of the host granite in the basic septum and vice versa, indicating a partially molten state of the host granite during the injection of the basic magma (e.g., Poli and Tommasini, 1991; Tommasini and Poli, 1992). A stratified basic complex outcrops in this sector of the Batholith near Capo Carbonara (CCB, Fig. 1), and along contacts with the surrounding granite shows mechanical interaction phenomena similar to those found between the BS and the host granites.

Petrography and mineral chemistry—The GP consist of medium- to coarse-grained granodiorites with hypidiomorphic heterogranular textures due to K-feldspars megacrysts. The main minerals are quartz + plagioclase + K-feldspar + biotite ± amphibole, whilst accessory phases are oxides + apatite + zircon ± titanite ± allanite.

MME vary in composition from gabbros and diorites to tonalites, and generally have fine-grained hypidiomorphic equigranular textures, although ophitic textures are present in the least evolved samples. Xenocrysts and rounded fragments of the host granite, from millimeters up to a few centimeters in size, are ubiquitous in hand specimen. The main minerals are quartz + plagioclase ± K-feldspar + biotite ± amphibole ± clinopyroxene, whilst accessory phases are oxides + apatite + zircon ± titanite ± allanite.

The CCB and the BS consist of medium-grained amphibole-bearing gabbros and quartz-gabbros with autoallotriomorphic and intergranular textures. The latter texture provides evidence for the occurrence of cumulus processes within the CCB and BS. In the outer sectors both the BS and CCB have medium-to fine-grained porphyritic textures with glomerocrystals of plagioclase and amphibole. The main minerals are plagioclase + amphibole + quartz ± biotite ±

Table 1
Selected plagioclase analyses of the Sarrabus calc-alkaline association

	CCB_{inn}		CCB_{out}		BS_{inn}		BS_{out}		MMEg		GP	
	Core	Rim	Core	Rim	Core	Rim	Core	Rim	Core	Rim	Core	Rim
SiO_2	46.44	54.25	52.64	54.23	48.50	48.33	47.25	54.61	56.90	57.91	58.42	58.60
TiO_2	bdl	bdl	0.05	bdl	bdl	0.09	bdl	bdl	0.02	0.05	0.02	0.04
Al_20_3	34.34	28.68	29.69	28.72	32.88	33.10	33.04	28.56	26.21	26.01	25.77	25.90
Fe_20_3	0.13	0.13	0.20	0.21	0.53	0.20	0.48	0.17	0.12	0.14	0.18	0.16
CaO	17.21	10.91	12.08	11.02	15.63	15.93	16.16	11.22	9.03	8.53	7.99	8.05
Na_20	1.69	5.21	4.53	5.23	2.64	2.31	2.06	5.14	6.15	6.54	6.81	6.76
K_20	0.04	0.10	0.04	0.06	0.07	0.07	bdl	0.05	0.14	0.28	0.38	0.33
SrO	0.09	0.34	0.31	0.11	0.15	0.65	0.32	0.12	0.32	0.10	0.05	0.07
Total	99.94	99.62	99.54	99.58	100.40	100.68	99.31	99.87	98.89	99.56	99.62	99.91
Si	2.137	2.461	2.398	2.459	2.215	2.206	2.186	2.468	2.583	2.606	2.625	2.624
Al	1.862	1.533	1.594	1.535	1.770	1.781	1.801	1.521	1.402	1.380	1.365	1.367
Ti	–	–	0.002	–	–	0.003	–	–	0.001	0.002	0.001	0.001
Fe^{3+}	0.005	0.004	0.007	0.007	0.018	0.007	0.020	0.006	0.004	0.005	0.006	0.005
Ca	0.848	0.530	0.590	0.535	0.765	0.779	0.801	0.543	0.439	0.411	0.384	0.386
Na	0.151	0.458	0.400	0.460	0.234	0.204	0.185	0.450	0.541	0.571	0.593	0.587
K	0.002	0.006	0.002	0.003	0.004	0.004	–	0.003	0.008	0.016	0.022	0.019
Sr	0.002	0.009	0.008	0.003	0.004	0.017	0.009	0.003	0.008	0.003	0.001	0.002
Ab	15.08	46.08	40.32	46.09	23.33	20.67	18.74	45.19	54.75	57.18	59.37	59.18
An	84.72	53.32	59.48	53.61	76.27	78.93	81.26	54.52	44.43	41.21	38.47	38.95
Or	0.20	0.60	0.20	0.30	0.40	0.41	0.00	0.29	0.82	1.61	2.15	1.88

bdl = below detection limit.

clinopyroxene, whilst accessory phases are oxides + apatite + titanite ± zircon. The samples of the CCB and BS have been grouped in: (i) samples representative of the inner facies (CCB_{inn} and BS_{inn}) and (ii) samples representative of the outer facies (CCB_{out} and BS_{out}), within a few meters of the contact with the host granite. MME have been grouped on the basis of their composition: (i) gabbro-diorites (MMEg) and (ii) tonalites (MMEt).

Representative analyses of the main mineral phases are reported in Tables 1–4. Plagioclase is euhedral to subeuhedral with tabular shape, is zoned and twinned following Albite law. It is noteworthy that plagioclases have patchy zoning textures in the mafic enclaves and in the outer facies of the CCB and BS, with a compositional range from An_{85} to An_{44} (cores), and from An_{55} to An_{35} (rims) (Table 1).

Amphibole has mainly subeuhedral habitus and shows colors of pleochroism from brownish to green; sometimes it has anhedral habitus and is present as poikilitic crystals; remnants of clinopyroxene are commonly found in the core of amphiboles. Composition is quite variable and strictly coupled with bulk-rock chemistry and mineral-forming process (Table 2, Fig. 2). Amphibole of the inner facies of the CCB and BS vary from pargasite to Mg-hornblende, establishing a tschermakite-type substitution. Amphiboles forming rims around clinopyroxene show a different well defined trend towards actinolite composition, indicating an origin by reaction between clinopyroxene and liquid (e.g., Nakajima

Table 2
Selected amphibole analyses of the Sarrabus calc-alkaline association

	CCB_{inn}		CCB_{out}		BS_{inn}		BS_{out}		MMEg	MMEt	GP	
	MgHb	AcHb	FeHb	FEd	FPaHb	AcHb	MgHb	MgHb	FEd	FEd	FEd	FEdHb
SiO_2	48.66	50.95	45.86	43.64	42.08	51.48	45.32	46.30	45.30	43.82	43.61	43.27
TiO_2	0.73	0.57	1.36	1.41	2.48	0.43	1.14	1.02	1.08	1.22	1.42	1.44
Al_20_3	6.52	4.65	8.15	8.93	11.75	4.37	8.57	8.36	7.26	8.11	8.50	8.46
Cr_20_3	0.08	0.06	0.04	0.04	0.12	0.27	0.16	0.10	bdl	0.14	bdl	bdl
Fe_20_3	2.82	2.63	0.14	2.50	bdl	0.49	1.29	0.15	bdl	1.01	0.06	1.16
FeO	10.65	9.31	17.95	17.28	14.79	10.76	17.01	17.58	19.37	19.26	20.30	19.31
MnO	0.33	0.32	0.95	0.58	0.35	0.40	0.53	0.51	0.81	0.71	0.75	0.67
NiO	0.13	bdl	0.10	bdl	bdl	bdl	bdl	0.06	0.08	bdl	bdl	0.12
MgO	15.23	17.19	10.22	9.26	12.23	16.28	10.71	10.92	9.46	8.79	8.33	8.52
CaO	11.37	11.43	11.46	11.92	10.49	11.69	10.79	10.55	11.31	11.23	11.29	11.32
Na_20	0.71	0.67	1.18	1.02	2.27	0.64	1.09	0.98	1.30	1.20	1.24	1.24
K_20	0.37	0.19	0.71	1.11	0.51	0.00	0.43	0.36	0.89	0.98	1.18	1.05
Total	97.59	97.97	98.11	97.69	97.07	96.81	97.04	96.90	96.86	96.47	96.69	96.56
Si	7.069	7.291	6.877	6.635	6.310	7.449	6.827	6.954	6.945	6.776	6.753	6.702
Al^{IV}	0.931	0.709	1.123	1.365	1.690	0.551	1.173	1.046	1.055	1.224	1.247	1.298
Al^{VI}	0.185	0.076	0.317	0.235	0.387	0.194	0.348	0.433	0.257	0.253	0.304	0.247
Ti	0.080	0.061	0.153	0.161	0.280	0.047	0.129	0.115	0.125	0.142	0.165	0.168
Fe^{3+}	0.309	0.283	0.016	0.286	–	0.053	0.146	0.016	–	0.117	0.006	0.136
Cr	0.009	0.007	0.005	0.005	0.014	0.031	0.019	0.012	–	0.017	–	–
Mg	3.298	3.667	2.285	2.099	2.734	3.512	2.405	2.445	2.162	2.026	1.923	1.967
Ni	0.015	–	0.012	–	–	–	–	0.007	0.010	–	–	0.015
Fe^{2+}	1.293	1.115	2.250	2.197	1.855	1.302	2.143	2.208	2.484	2.491	2.629	2.501
Mn	0.041	0.039	0.121	0.075	0.044	0.049	0.068	0.065	0.105	0.093	0.098	0.088
Ca	1.770	1.753	1.841	1.942	1.685	1.812	1.741	1.698	1.858	1.860	1.873	1.879
Na	0.200	0.186	0.343	0.301	0.660	0.180	0.318	0.285	0.386	0.360	0.372	0.372
K	0.069	0.035	0.136	0.215	0.098	–	0.083	0.069	0.174	0.193	0.233	0.207
A-site	0.27	0.22	0.48	0.52	0.76	0.18	0.40	0.35	0.56	0.55	0.61	0.58
Mg#	0.67	0.72	0.49	0.45	0.59	0.71	0.51	0.52	0.46	0.43	0.41	0.42

MgHb: magnesio hornblende; AcHb: actinolitic hornblende; FeHb: ferroan hornblende; FEdHB: ferroan edenitic hornblende; FPaHb: ferroan pargasitic hornblende; FEd: ferroan edenitic. bdl = below detection limit.

Table 3
Selected biotite analyses of the Sarrabus calc-alkaline association

	CCB_{inn}		CCB_{out}		MMEg	MMEt	GP	
SiO_2	35.83	35.92	36.01	35.17	35.82	36.06	35.87	35.69
TiO_2	3.00	3.68	3.66	3.79	3.31	3.90	3.95	2.96
Al_20_3	15.29	15.01	14.66	14.90	14.79	14.75	13.96	14.66
Cr_20_3	0.04	0.07	0.06	bdl	0.02	0.04	bdl	bdl
FeO	20.27	21.01	22.12	22.54	22.61	22.45	23.32	23.45
MnO	0.16	0.19	0.53	0.30	0.32	0.34	0.20	0.76
NiO	bdl	bdl	0.09	bdl	bdl	0.10	bdl	0.13
MgO	11.07	10.92	9.39	9.42	9.15	8.45	8.75	8.70
N_20	0.33	0.28	0.00	0.17	0.06	0.04	0.09	bdl
K_20	9.45	9.65	9.81	9.48	9.85	9.81	9.72	9.81
BaO	0.45	0.51	0.28	0.54	0.08	0.37	0.33	0.18
Total	95.89	97.24	96.61	96.31	96.01	96.31	96.19	96.35
Si	5.498	5.464	5.544	5.451	5.550	5.575	5.578	5.552
Al^{IV}	2.502	2.536	2.456	2.549	2.450	2.425	2.422	2.448
Al^{VI}	0.264	0.155	0.204	0.172	0.251	0.263	0.136	0.240
Ti	0.346	0.421	0.424	0.442	0.386	0.453	0.462	0.346
Cr	0.005	0.008	0.007	0.000	0.002	0.005	–	–
Fe	2.601	2.673	2.848	2.921	2.930	2.903	3.032	3.051
Mn	0.021	0.024	0.069	0.039	0.042	0.045	0.027	0.101
Ni	–	–	0.011	–	–	0.013	–	0.016
Mg	2.532	2.476	2.155	2.176	2.114	1.947	2.028	2.019
Na	0.098	0.083	0.000	0.051	0.018	0.012	0.028	0.000
K	1.850	1.873	1.927	1.874	1.947	1.935	1.928	1.947
Ba	0.027	0.030	0.017	0.033	0.005	0.023	0.020	0.011
Mg#	0.49	0.48	0.43	0.42	0.42	0.40	0.40	0.39

bdl = below detection limit.

and Ribbe, 1981). Amphibole of the outer facies of CCB and BS, along with amphibole occurring in mafic enclaves varies from Mg-hornblende to edenitic and Fe-edenitic hornblende. The decrease in Mg# is coupled with a decrease of Si atoms in the tetrahedral site along with an increase in A-site occupancy, demonstrating the occurrence of edenite-type substitution. These distinct compositional variations appear to be a general feature of amphibole-bearing rocks of the Sardinia–Corsica Batholith. As an example, amphiboles occurring in the Sarrabus samples are compared with those occurring in the Punta Falcone gabbroic complex (Fig. 2). The similar trends exhibited by amphiboles occurring in the rocks of these two sectors of the Sardinia–Corsica Batholith are striking, and establish a marked dependence of composition upon the mineral-forming process. In the inner facies, amphibole replacing clinopyroxene in the crystallisation sequence is displaced along actinolitic composition, whilst amphibole directly crystallising from the liquid (in response to the P_{H_2O}

Table 4
Selected ilmenite analyses of the Sarrabus calc-alkaline association

	CCB_{inn}		BS_{inn}		BS_{out}	
TiO_2	47.25	48.74	48.05	48.52	50.44	50.92
Al_20_3	0.02	0.03	0.15	0.11	bdl	0.03
Cr_20_3	bdl	0.07	0.03	0.08	bdl	bdl
Fe_20_3	9.30	8.53	8.16	6.62	4.24	3.14
FeO	39.19	37.40	37.61	41.86	42.45	42.92
MnO	3.02	6.01	4.92	1.54	2.64	2.83
NiO	bdl	bdl	0.11	bdl	0.04	bdl
MgO	0.09	0.14	0.12	0.12	0.11	bdl
CaO	0.06	0.07	0.23	bdl	bdl	bdl
Total	98.93	100.99	99.38	98.84	99.91	99.84
Al	0.001	0.001	0.004	0.003	–	0.001
Cr	–	0.001	0.001	0.002	–	–
Fe^{3+}	0.179	0.161	0.156	0.127	0.081	0.06
Ti	0.91	0.918	0.919	0.934	0.96	0.97
Mg	0.003	0.005	0.005	0.005	0.004	–
Ni	–	–	0.002	–	0.001	–
Fe^{2+}	0.839	0.784	0.800	0.896	0.898	0.909
Mn	0.066	0.128	0.106	0.033	0.057	0.061
Ca	0.002	0.002	0.006	–	–	–

Fe_2O_3 determined by stoichiometry. bdl = below detection limit.

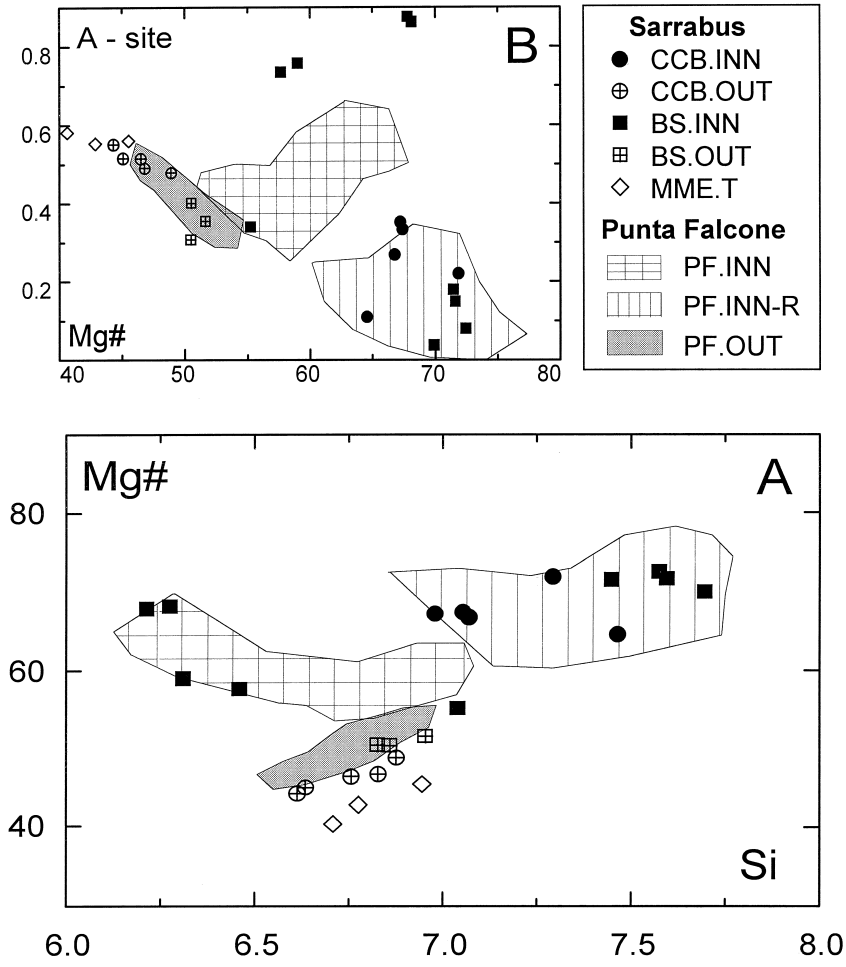

Fig. 2. Calcic amphiboles of the Sarrabus basic complexes (CCB and BS), mafic enclaves (MMEt), and the Punta Falcone basic complex. (A) Atoms of Si p.f.u. vs. Mg# [$Mg^{2+}/(Mg^{2+} + Fe^{2+})$ mol%]; (B) A-site occupancy vs. Mg#. CCB.INN and CCB.OUT: inner and outer facies of the Capo Carbonara basic complex, respectively. BS.INN and BS.OUT: inner and outer facies of the basic septa, respectively. MME.T: tonalitic mafic enclave. PF.INN: Punta Falcone magmatic amphiboles (basic liquid → amphibole); PF.INN-R: Punta Falcone reaction amphiboles (cpx + liquid → amphibole); PF.OUT: Punta Falcone interaction amphiboles (contaminated basic liquid → amphibole) (Tommasini and Poli, 1992).

increase caused by crystallisation of anhydrous phases) has pargasitic composition. Finally, in the outer facies and in the enclaves, amphibole crystallising from the 'basic' liquid, which is being contaminated by the host granite magma (CFC process, Poli and Tommasini, 1991), exhibits a trend towards edenitic composition.

Biotite is present only in the outer facies of the BS, whereas is ubiquitous in all of the CCB facies, with increasing modal proportions approaching the contacts with the host granite. Biotite has subeuhedral habitus, pleochroic colors from dark- to pale-brown and a composition corresponding to a solid solution of equal amounts of annitic, phlogopitic, siderophillitic, and eastonitic components (Mg# = 0.42–0.49, Al^{IV} = 2.45–2.55 a.f.u., Table 3).

Quartz is anhedral and occurs as interstitial phase. K-feldspar is sometimes present as interstitial phase in the CCB, BS, and enclaves. Ilmenite is widespread in the CCB and BS (Table 4).

3. Geochemistry

Representative chemical analyses of the different intrusive rocks outcropping in this sector of southeastern Sardinia are reported in Table 5. Overall the samples define a subalkaline association and, in particular, a calc-alkaline association with normal and high contents of K_2O (0.47–2.43 wt.%), with the exception of the MMEg ($K_2O = 2.10–3.72$ wt.%), which plot within the field of alkaline series (ALK = 7.26–5.53 wt.%).

Major element variation diagrams are reported in Fig. 3A. The samples of the GP are relatively homogeneous and define distinct fields from the samples of the CCB and BS. The least evolved granite sample (SP214, Table 5), collected along the contact with the CCB, has a major element composition similar to that of the tonalitic mafic enclaves (MMEt). The MMEt have intermediate compositions between the host granites and the basic complexes (BS and CCB). The gabbro-dioritic mafic enclaves (MMEg) and the outer facies of the basic complexes (BS_{out} and CCB_{out}) exhibit on average higher Fe_2O_3, TiO_2 and P_2O_5 than the other samples, while SiO_2 is similar to that of the inner facies of the BS and CCB.

On trace element variation diagrams (Fig. 3B), the GP, excluding sample SP214, still have a relatively homogeneous composition, with the exception of Ba content. On the other hand, the MMEt do not show intermediate compositions among the two groups of rocks, suggesting a complex genetic history. The MMEg and the outer facies of the CCB and BS have higher contents of some trace elements with large ionic radius and high field strength (e.g., Rb, Ba, Y, Nb) than the MMEt and the inner facies of the CCB and BS.

Chondrite-normalised rare earth elements (REE) diagrams are reported in Fig. 4. The comparison between the REE patterns of the samples of the inner and outer facies of the CCB and BS indicates that: (i) there is a clear similarity between REE patterns of the inner and outer facies in the CCB and BS; (ii) the absolute contents of REE are systematically lower in the inner facies; (iii) the fractionation of the light rare earths (LREE) tends to decrease in the outer facies whereas the negative anomaly of Eu tends to increase; (iv) the heavy rare earths (HREE) are not significantly fractionated although the outer facies have on the average $(Tb/Yb)_n$ values slightly higher than one; (v) the inner facies have REE patterns typical of calc-alkaline basalts (e.g., Wilson, 1989). The decrease of LREE fractionation along with the higher REE content in the outer facies suggest the occurrence of some process of accumulation of middle REE-bearing minerals (e.g., amphibole, titanite).

The two groups of mafic enclaves have completely different REE patterns: (i) the MMEg have unfractionated LREE with absolute contents lower than the MMEt; (ii) the MMEt exhibit a significant fractionation of the LREE ($La/Sm = 6–8$); (iii) the negative Eu anomaly, present in both groups, tends to be more accentuated in the MMEg; (iv) the HREE contents are systematically higher in the MMEg (Yb up to $35 \times$ chondrite), whereas their fractionation, substantially uniform, does not show any significant difference between the two groups of enclaves. Again, the fairly flat REE pattern of the MMEg, with the exception of the negative Eu anomaly, is suggestive of accumulation of middle REE-bearing minerals along with fractionation of plagioclase. The REE content and pattern of the GP is similar to that of the tonalitic mafic enclaves (MMEt).

Initial isotopic ratios (Table 6) have been calculated at 300 Ma on the basis of K/Ar radiometric dating (Nicoletti et al., 1982) on a granodiorite of Capo Carbonara. Such a calculation is supported by field evidence suggesting that the CCB, the BS, and MME were injected into a still partially molten granite magma (GP), thus sharing a common cooling history. It is clear that the mafic enclaves and the GP have quite similar initial isotopic values, while the sample of the BS has a less marked crustal signature both for Sr and Nd.

4. Discussion

A petrogenetic model explaining differentiation processes which formed the different basic facies outcropping in this sector of southeastern Sardinia, must take into account field, petrographic, and geochemical data, namely: (i) the relative surface area of outcrop of the different intrusive facies, e.g., the relative abundance of acid and basic rocks, and the surrounding geologic context (Fig. 1); (ii) the geochemical differences and similarities between the

Table 5
Representative analyses of major (wt.%) and trace (ppm) elements of the Sarrabus calc-alkaline association

Sample	Basic complex of Capo Carbonara								Basic septa			
	Inner facies					Outer facies			Inner facies		Outer facies	
	ga SP207	ga SP209	qz-ga SP201	qz-di SP210	qz-di SP208	qz-ga SP227	qz-ga SP213	ton SP206	qz-ga SP230	ga SP236	qz-ga SP228	qz-ga SP229
SiO_2	48.88	49.95	51.33	52.25	53.92	48.59	51.19	58.58	47.59	47.88	47.48	48.70
TiO_2	0.74	0.96	0.99	0.34	0.62	1.53	1.9	1.19	0.87	0.98	1.39	1.59
Al_2O_3	17.37	14.32	17.77	19.70	18.13	18.33	19.07	17.00	17.84	16.02	19.30	19.16
Fe_2O_3	9.77	14.33	9.53	6.83	8.03	12.01	11.21	8.92	9.59	10.59	12.05	11.23
MnO	0.10	0.14	0.10	0.09	0.09	0.11	0.10	0.09	0.10	0.10	0.11	0.11
MgO	8.22	7.72	5.47	5.06	4.60	4.45	2.48	2.26	7.06	8.93	4.84	4.41
CaO	10.11	8.26	9.82	12.77	10.10	9.12	8.69	6.42	12.65	10.74	10.14	8.57
Na_2O	1.57	0.81	1.93	1.09	1.79	2.39	1.97	2.02	1.63	2.10	2.19	2.39
K_2O	0.92	1.22	1.24	0.69	0.97	1.52	2.06	2.10	0.80	0.47	1.37	1.67
P_2O_5	0.15	0.18	0.23	0.14	0.17	0.34	0.49	0.25	0.22	0.30	0.32	0.35
LOl	2.16	2.12	1.60	1.04	1.58	1.61	0.84	1.16	1.62	1.88	0.81	1.83
Total	99.99	100.01	100.01	100.00	100.00	100.00	100.00	99.99	100.00	99.99	100.00	100.01
Sc	–	–	–	29	30	35	36	26	43	34	48	32
V	251	202	245	112	168	243	264	195	226	176	260	254
Cr_{XRF}	342	823	83	448	190	15	19	25	216	379	30	27
Cr_{INAA}	–	–	–	528	222	16	19	32	243	429	26	27
Co_{XRF}	38	55	29	27	29	30	19	18	30	41	25	24
Co_{INAA}	–	–	–	29	27	26	18.5	17.6	29	41	24	23
Ni	42	170	13	52	28	13	11	9	13	142	11	12
Rb	44	67	57	34	43	72	76	88	20	14	49	74
Sr	226	164	244	243	252	303	343	245	385	381	333	351
Y	12	17	29	10	20	45	51	35	24	20	62	43
Zr	54	51	75	51	72	204	355	175	89	142	211	250
Nb	5	6	11	3	7	15	20	12	5	10	14	16
Ba	193	309	259	126	192	556	1042	529	169	247	700	661
Hf	–	–	–	1.2	2.1	4.8	7.8	–	2	2.5	5.1	5.7
Ta	–	–	–	0.28	0.57	0.67	1	–	0.24	0.47	0.57	0.89
Th_{XRF}	2.5	2.5	5.3	2.9	3.7	1.4	7.3	3	2.9	3.6	1.5	4.3
Th_{INAA}	–	–	–	4.3	5.6	3.8	7.1	–	1.6	2.4	2.3	2.9
La_{XRF}	9	6	19	9	15	29	39	20	11	18	29	30
Ce_{XRF}	13	10	48	15	28	63	92	40	20	35	72	66
La_{INAA}	–	–	–	10.3	17.6	31	45	22	11	20.1	33	31
Ce_{INAA}	–	–	–	18.9	38	69	94	48	20	40	78	67
Nd	–	–	–	7.5	20.3	36	50	27	14.6	19.8	46	37
Sm	–	–	–	2	4.6	8.8	12.9	7.4	4.2	4.8	13.4	9.3
Eu	–	–	–	0.57	0.92	1.8	2.03	1.4	1.04	1.2	2.15	1.77
Tb	–	–	–	0.29	0.7	1.02	1.57	1.1	0.55	0.46	1.88	1.18
Yb	–	–	–	0.7	1.9	3.8	4.4	3.5	2	1.8	5.3	3.5
Lu	–	–	–	0.2	0.32	0.61	0.68	0.53	0.32	0.32	0.77	0.53
$(Tb/Yb)_n$	–	–	–	1.6	1.5	1.1	1.45	1.25	1.15	1.04	1.45	1.38
Eu/Eu*	–	–	–	0.98	0.67	0.82	0.6	0.66	0.93	1.1	0.57	0.71
∑REE	–	–	–	47	101	178	249	135	76	101	222	180

ga: gabbro; qz-ga: quartz-gabbro; qz-di: quartz-diorite; ton: tonalite; gd: granodiorite.
–: not determined. Major elements (exclusive of Na_2O, MgO, and LOI determined by wet chemical analyses) analysed by XRF with full matrix correction after Franzini and Leoni (1972); V, Cr_{XRF}, Co_{XRF}, Ni, Rb, Sr, Y, Zr, Nb, Ba, and Th_{XRF} by XRF after Kaye (1965); Sc, Cr_{INAA}, Co_{INAA}, Hf, Ta, Th_{INAA}, and REE by INAA (Poli et al., 1977). The precision is better than 15% for V, Cr_{INAA}, Ni, Tb, and Lu better than 10% for Co_{XRF}, Cr_{XRF}, Y, Zr, Ba, Ta, and Yb, and better than 5% for all the other elements. The accuracy has been tested on international standards and is better than 10%.

Sample	Microgranular mafic enclaves					Granites		
	MMEg		MMEt					
	qz-ga SP238	qz-di SP219	ton SP218	ton SP242	ton SP232	gd SP214	gd SP237	gd SP241
SiO_2	51.49	52.08	60.33	61.31	65.1	64.13	67.4	67.75
TiO_2	1.33	1.26	1.35	1.06	0.73	0.80	0.53	0.48
Al_2O_3	18.37	17.33	16.94	16.64	15.91	16.20	15.98	15.93
Fe_2O_3	11.88	11.38	7.81	7.55	5.75	5.68	4.16	3.76
MnO	0.14	0.13	0.07	0.09	0.08	0.07	0.06	0.06
MgO	3.49	3.88	2.23	2.17	1.89	1.77	1.17	1.13
CaO	5.64	7.5	4.58	4.13	4.21	4.10	3.55	3.32
Na_2O	3.7	3.43	3.15	3.44	3.52	3.04	3.47	3.37
K_2O	3.01	2.1	2.43	2.42	1.81	3.33	2.87	3.45
P_2O_5	0.25	0.28	0.3	0.22	0.18	0.19	0.18	0.16
LOI	0.7	0.63	0.81	0.98	0.82	0.69	0.63	0.60
Total	100.00	100.00	100.00	100.01	100.00	100.00	100.00	100.01
Sc	47	32	21.4	13.1	–	18.5	9.1	11.3
V	245	230	151	130	110	100	68	60
Cr_{XRF}	36	39	12	6	5	15	4	2
Cr_{INAA}	37	39	17	12	–	20	10	7
Co_{XRF}	23	23	14	14	13	10.2	8	7
Co_{INAA}	21	19.9	13.9	19.2	–	10.2	7.4	7.1
Ni	21	14	11	11	10	7	8	9
Rb	210	145	153	189	149	138	131	135
Sr	148	189	201	171	168	207	190	187
Y	76	45	24	32	31	38	21	21
Zr	209	188	297	207	167	218	178	158
Nb	22	19	18	20	14	12	11	8
Ba	527	286	553	483	351	910	603	812
Hf	5.1	4.6	6.8	4.5	–	5.4	4.2	3.9
Ta	1.92	1.24	0.98	1.68	–	0.94	0.88	0.7
Th_{XRF}	3.5	2	16.6	10.8	13.5	13.8	9	15.2
Th_{INAA}	6.9	1.8	14.1	12.1	–	16.1	11	14.4
La_{XRF}	21	14	47	32	35	40	25	44
Ce_{XRF}	38	32	105	60	63	88	50	85
La_{INAA}	20.6	15.7	56	34.4	–	49	31	46
Ce_{INAA}	42	39	104	62	–	92	54	83
Nd	22.2	25.9	38	24.7	–	38	23.8	30.7
Sm	9.5	8.4	7.3	5.4	–	8.9	4.6	5.7
Eu	1.19	1.4	1.16	0.94	–	1.28	1	1.08
Tb	1.98	1.17	0.73	0.83	–	1.24	0.54	0.71
Yb	6.6	4.5	2	2.9	–	3.2	2	1.9
Lu	1.01	0.74	0.31	0.44	–	0.46	0.32	0.34
$(Tb/Yb)_n$	1.22	1.05	1.48	1.17	–	1.60	1.13	1.57
$Eu/Eu*$	0.37	0.61	0.66	0.6	–	0.50	0.86	0.7
ΣREE	145	123	233	153	–	225	132	190

inner and outer facies of the CCB and BS, and between the two groups of mafic enclaves (MMEt and MMEg, Figs. 3 and 4); (iii) the geochemical evidence (REE, Fig. 4) for the occurrence of cumu-

lus processes in the MMEg and in the outer facies of the CCB and BS, which is not coupled with a clear textural evidence; (iv) the relatively homogenous composition of the host granites (GP), excluding sample SP214 (Table 5, Figs. 3 and 4); (v) the presence of plagioclase with patchy zoning textures in the mafic enclaves and in the outer facies of the CCB and BS; (vi) the peculiar compositional variations of the different amphibole types (Fig. 2) depending upon the mineral-forming process.

A single genetic process starting from a parental basic magma (e.g., crystal fractionation) is not able

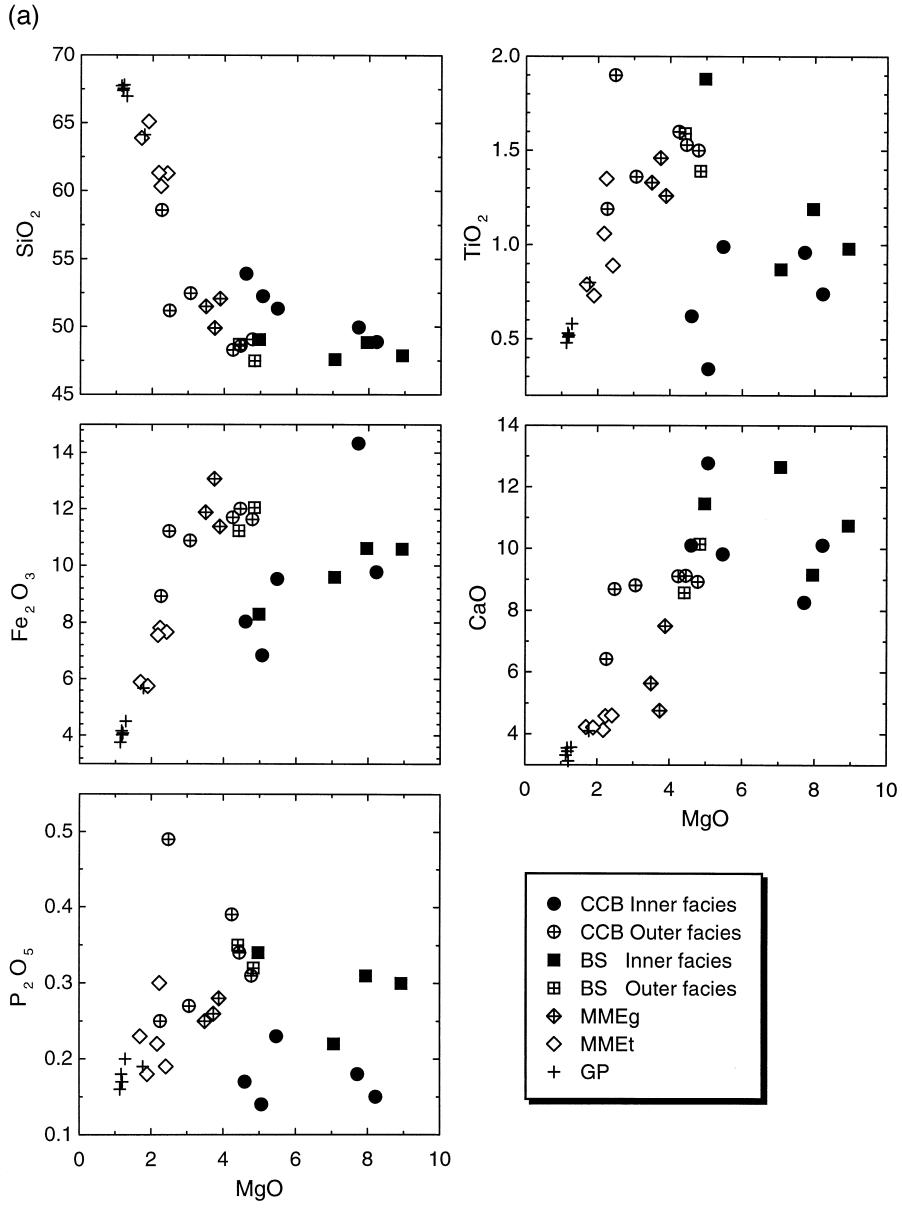

Fig. 3. Harker diagrams illustrating the main trends exhibited by the Sarrabus calc-alkaline association for major (A) and trace elements (B). CCB: Capo Carbonara basic complex; BS: basic septa; MMEg: gabbro-dioritic microgranular mafic enclaves; MMEt: tonalitic microgranular mafic enclaves; GP: granite plutons.

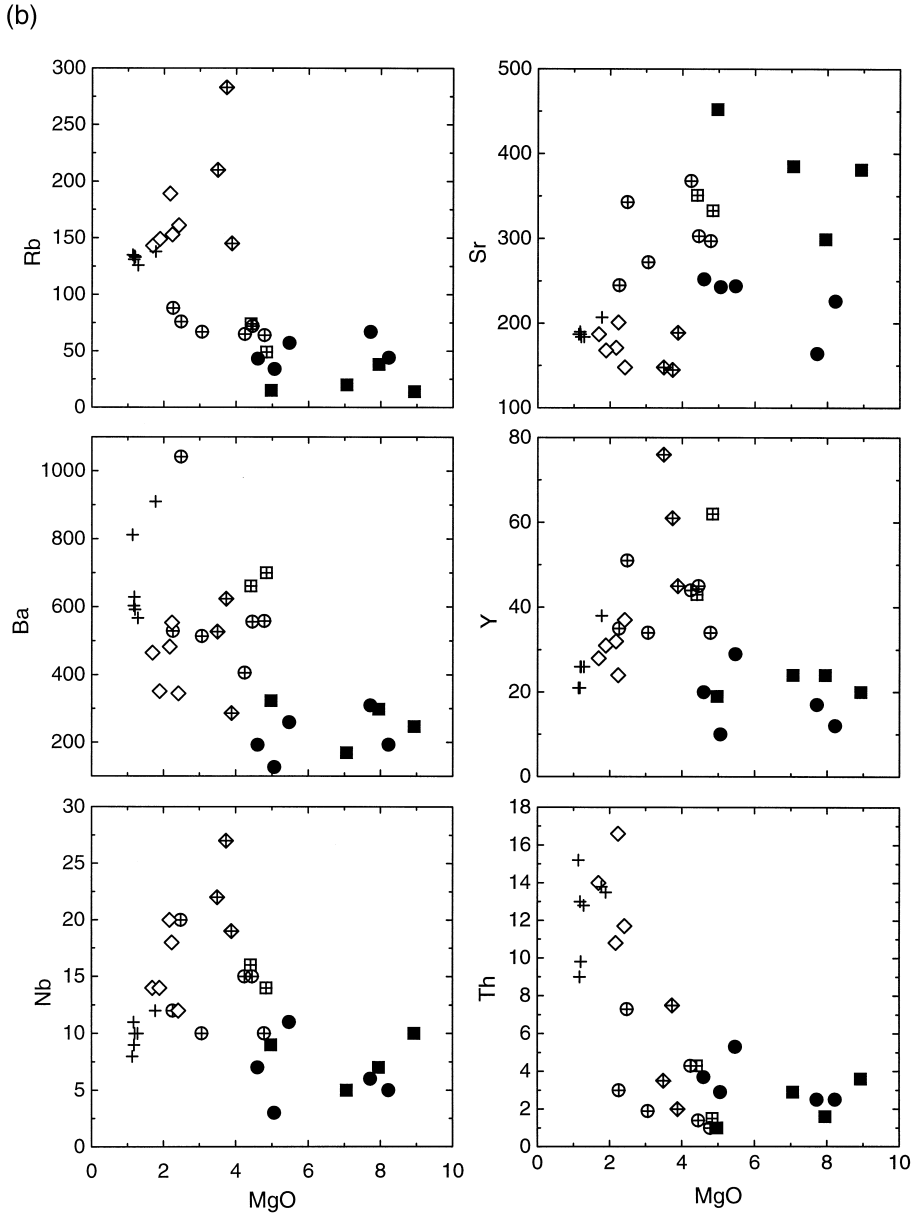

Fig. 3 (continued).

to explain the formation of all the Sarrabus intrusive rocks. In particular, mass balance arguments would require special pleading in order to satisfy the observed proportions of acid (> 95%) and basic (< 5%) rocks. Thus, on the basis of previous works (Poli et al., 1989; Tommasini et al., 1995), we consider that acid and basic magmas are derived from different sources and, following injection of the basic magmas into still partially molten acid magmas, gave rise to physico-chemical interactions. In the remainder of the discussion, we try to unravel differentiation processes of the basic and intermediate-acid facies sepa-

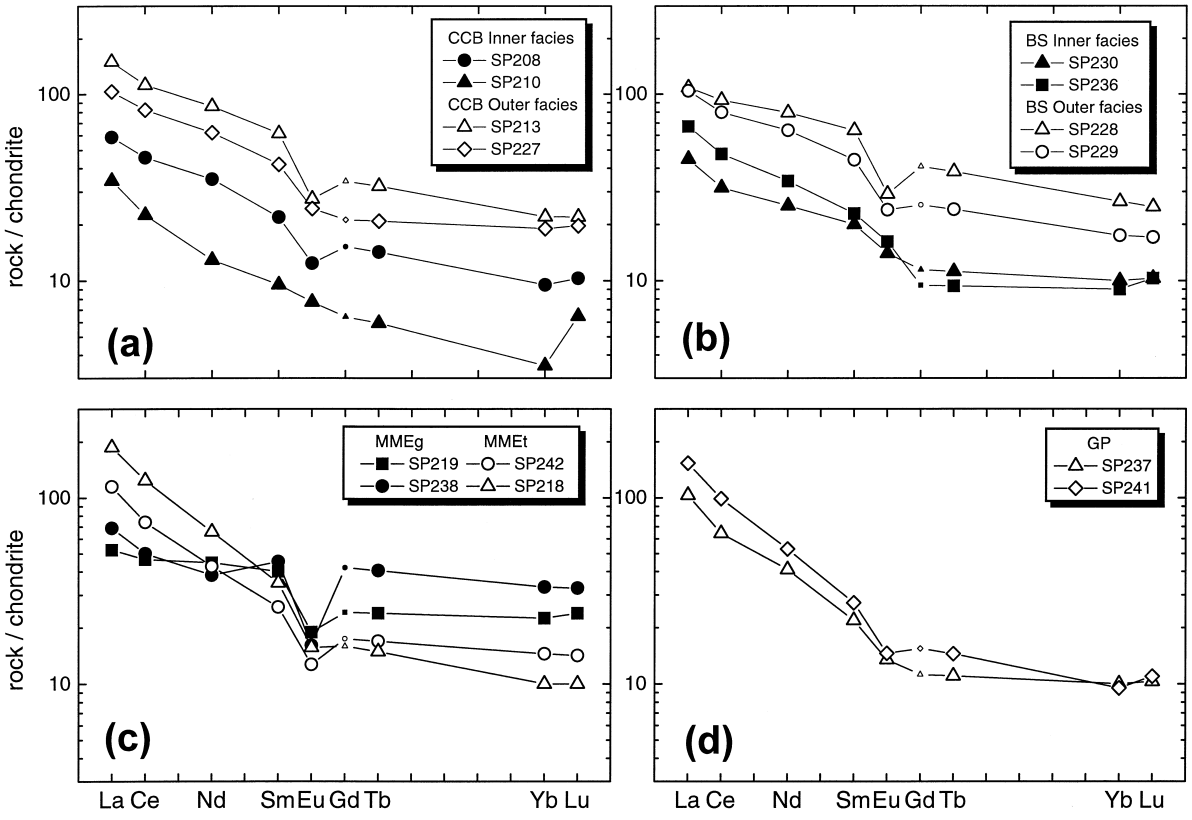

Fig. 4. Chondrite-normalised (Haskin et al., 1966) REE patterns of the CCB (A), BS (B), MME (C), and GP (D). Normalised values of Gd are interpolated.

rately, with the aim of understanding the genetic relationships between these two groups of rocks and enclaves.

4.1. Differentiation processes of the inner facies of the CCB and BS

The texture of the inner facies of the CCB as well as their geochemical characteristics, e.g., Al_2O_3, Sr, MgO, Ni, Cr contents (Table 5), indicate that cumulus of amph + cpx + plg and trapping of residual liquid has been the main differentiation process. This implies that the chemical composition of the samples is not likely to be representative of magmatic liquids (e.g., Wager and Brown, 1967; Irvine, 1979; Irvine, 1980; Cawthorn, 1996). Tommasini and Poli (1992) developed a geochemical model for cumulus–intercumulus processes in the basic complex of Punta Falcone, northern Sardinia, and established that the formation of the different gabbroic units could be modeled by adding to the parental magma an appropriate amount of early-crystallised minerals. The extensive cover in the outcropping sector of the CCB does not permit a detailed geological mapping, hence it is not possible to estimate the parental magma composition by outcropping surface mass balance. A linear computation program (e.g., Wright and Doherty, 1970) was then chosen leaving as unknown the parental magma composition in addition to the amounts of early-crystallised minerals. Being the linear system overestimated, the constraint used was to minimise the sum of squares of residuals. This mathematical model has been applied to the samples of the inner facies of the CCB assuming a single step of crystallisation (Table 7). The model does not converge to reasonable results using a primitive

Table 6
Sr and Nd isotope data of representative samples of the Sarrabus calc-alkaline association

Sample	Unit	Rb	Sr	$^{87}Rb/^{86}Sr$	$^{87}Sr/^{86}Sr 2\sigma$	$^{87}Sr/^{86}Sr_i$	Nd	Sm	$^{147}Sm/^{144}Nd$	$^{143}Nd/^{144}Nd 2\sigma$	$^{143}Nd/^{144}Nd_i$
SP230	BS	17.53	357.4	0.1419	0.707301 ± 14	0.70670 ± 2	15.24	3.704	0.1469	0.512325 ± 09	0.51204 ± 1
SP218	MMEt	143.2	189.0	2.195	0.718139 ± 11	0.70877 ± 1	36.85	6.068	0.0995	0.512151 ± 08	0.51196 ± 1
SP219	MMEg	133.5	179.2	2.157	0.717774 ± 17	0.70857 ± 2	28.46	7.306	0.1552	0.512268 ± 09	0.51196 ± 1
SP238	MMEg	207.1	143.9	4.174	0.726719 ± 09	0.70890 ± 1	25.82	8.578	0.2009	0.512352 ± 09	0.51196 ± 1
SP237	GP	128.0	186.6	1.986	0.717457 ± 10	0.70898 ± 1	21.75	4.186	0.1163	0.512206 ± 08	0.51198 ± 1
SP241	GP	128.0	185.0	2.004	0.717325 ± 13	0.70877 ± 1	29.97	5.265	0.1062	0.512168 ± 10	0.51196 ± 1

Sr and Nd isotopic analyses were normalised to $^{86}Sr/^{88}Sr = 0.1194$ and $^{146}Nd/^{144}Nd = 0.7219$, respectively. Repeated analyses of SRM987 and La Jolla standards gave an average of $^{87}Sr/^{86}Sr$ of 0.71025 ± 1 (2σ, $n = 20$) and $^{143}Nd/^{144}Nd$ of 0.51185 ± 1 (2σ, $n = 20$), respectively. Initial isotopic ratios have been calculated at 300 Ma on the basis of K/Ar dating (Nicoletti et al., 1982). Uncertainties in measured and initial isotopic ratios refer to the least significant digits and represent 2σ run precision and 2σ error propagation, respectively. Isotopic analyses were performed at the University of Michigan using standard analytical procedures.

parental magma, whereas is satisfactory using an evolved parental magma. The computed parental magma composition is well within those found in the Sardinia–Corsica Batholith by Tommasini et al. (1995). In some samples (SP210 and SP208), however, the sum of squares of residuals is significantly >1, mainly due to the calculated SiO_2 content lower than that observed. This fact might be indicative of interaction processes with the host granite affecting also the inner sectors of the gabbroic complex.

The trace element composition of the parental magma and gabbroic facies was calculated using the amount of minerals obtained from the major element modeling along with K_ds values from Table 10. The results for a subset of trace elements are reported in Table 7, together with the calculated trace element composition of the parental magma. The calculated trace element contents match quite well those observed, and correlation coefficients between observed and calculated compositions are significant at 95% confidence-limit error.

The geochemical characteristics of the inner facies of the BS (Figs. 3 and 4, Table 5) indicate that these samples have undergone cumulus processes similar to those of the inner facies of the CCB. However, the different behaviour of some major and trace elements (TiO_2, alkalies, Rb, Sr, Zr) suggests that either the cumulus assemblage was different or the BS parental magma had a different degree of evolution prior to the intrusion in the crustal anatectic environment.

4.2. Differentiation processes of the outer facies of the CCB and BS and genetic relationships with the MME

The outer facies of the CCB and BS have higher contents of TiO_2, Fe_2O_3tot, P_2O_5 (Fig. 3A), lithophile (excluding Th) and high field strength elements

Table 7
Major and trace element modeling of the inner facies of the CCB complex

	SP207		SP209		SP201		SP210	SP208	Parental magma	
Parental magma	41.9		70.7		70.2		45.1	74.3	SiO_2	52.58
Plg (An_{85})	22.3		2.02		13.4		32.2	13.7	TiO_2	1.3
Clinopx	0		2.85		8.2		13.8	11.9	Al_2O_3	18.79
									Fe_2O_3	11.46
Amphibole	33.5		23.3		8.1		8.9	0	MnO	0.02
Magnetite	1.3		3.1		0		0	0	MgO	4.79
Total solid added	58.1		31.3		29.8		54.9	25.7	CaO	7.04
									Na_2O	1.72
Sum of squares of residuals	0.84		1.23		0.78		7.48	14.4	K_2O	1.94
									P_2O_5	0.34
	(*o*)	(*c*)	(*o*)	(*c*)	(*o*)	(*c*)				
Co	38	38.2	55	46	29	27			Co	38
Rb	44	49.7	67	55	57	55			Rb	44
Ba	193	233	309	238	259	248			Ba	193
Sr	226	255	164	156	244	201			Sr	226
Nb	5	5.6	6	5.9	11	9.8			Nb	5
Y	12	13.1	17	15.5	29	26			Y	12
Th	2.5	2.6	2.5	2.3	5.3	4.4			Th	2.5
La	9	8.5	6	6.4	19	16.2			La	9
r		0.999		0.9937		0.9954				
AED		7.1		7.4		8.7				

The amount (wt.%) of early-crystallised minerals added to the calculated parental magma to obtain the composition of the selected samples representative of the inner facies is reported (see Tommasini and Poli, 1992 for details). Estimation on water-free basis. Mineral compositions and partition coefficients are given in Table 9Table 10. P_2O_5 contents have been corrected for apatite (0.15% in all the rocks) on the basis of petrographic data. (*o*) observed values; (*c*) calculated values; *r*: linear correlation coefficient between calculated and observed composition; AED: average error deviations of the calculated composition.

(Fig. 3B) than the inner facies. Other important features are: (i) the SiO_2 content is not significantly different from that of the inner facies (Fig. 3); (ii) biotite is present in significant amounts (5–10%); (iii) plagioclase has a patchy zoning texture; (iv) REE patterns suggest the occurrence of cumulus of middle REE-bearing minerals such as amphibole, apatite, and titanite (see K_ds in Henderson, 1986). These geochemical features can be explained taking also into account the chemical compositions of the mafic enclaves. The gabbro-dioritic mafic enclaves (MMEg) have major element contents (Fig. 3A) and REE patterns (occurrence of accumulation of middle REE-bearing minerals, Fig. 4), that are indicative of similar differentiation processes to those occurred in the outer facies of the CCB and BS. Considering trace elements, however, there are some significant differences, notably the Rb and Sr content (Fig. 3B), that clearly distinguish the MMEg from the outer facies of the CCB and BS. On the other hand, the tonalitic mafic enclaves (MMEt) have more evolved compositions (Fig. 3, Table 5), and the REE patterns (Fig. 4) do not suggest the occurrence of cumulus processes.

According to the model proposed by Poli and Tommasini (1991) and Poli et al. (1996), the main evolutionary process experienced by basic magmas injected into acid magmas is crystal fractionation and contamination (CFC process), along with freezing, disruption and fragmentation of the basic magmas within the host acid magmas to eventually form the mafic enclaves. The mafic enclaves would then represent the final products of this complex physico-chemical process, and would record the evolutionary stages experienced by the basic magmas. Following this line of reasoning, we have tried to model a CFC process using the estimated parental magma of the CCB as starting composition and the most evolved granite sample as contaminant (Table 8).

The amounts of fractionated minerals have been obtained using the software MELTS (Ghiorso et al., 1994) in assimilation mode. For the sake of clarity, we have divided the process into two steps of crystallisation, averaging the fractionating mineral assemblages. The first step, up to F = 92%, is dominated by the crystallisation of oxide + clinopyroxene/amphibole (see caption of Fig. 5) + plagioclase, while the second step, up to F = 50–30%, is dominated by plagioclase with subordinate amounts of quartz + clinopyroxene/amphibole + K-feldspar + biotite + apatite. The two fractionating mineral assemblages were used to calculate the bulk distribution coefficients (D) for a set of trace elements, using K_d values in Tables 9 and 10. Thus, we obtained an independent line of evidence to verify whether trace element variations observed in the mafic enclaves and in the outer facies of the CCB and BS could be due to the CFC process envisaged by Poli and Tommasini (1991) and Poli et al. (1996) for acid–basic magma interaction.

The results of the computed CFC process are reported in Fig. 5. The modeled liquid line of descent generated by the two steps of CFC is able to reproduce the trend exhibited by the tonalitic mafic enclaves (MMEt), i.e., those enclaves that had no geochemical or textural evidence for the occurrence of cumulus processes. In contrast, the gabbro-dioritic mafic enclaves (MMEg) and the outer facies of the CCB and BS do not fit the liquid line of descent of the CFC process (Fig. 5). Their geochemical characteristics (Figs. 3 and 4), however, strongly suggest the occurrence of some kind of 'cumulus' process that did not leave textural evidence. In other words, we suggest that the genesis of these rocks could be

Table 8
Parameters of the CFC process used to model the differentiation of the MME and the outer facies of the BS and CCB

	C_0^a	C_a^b		MA (CFC 1)[c]	MA (CFC 2)[c]		D (CFC 1)[d]	D (CFC 2)[d]
Co	43	7	CPX	0.11	0.03	Co	4.69	1.74
Rb	45	135	HB	0.1	0.04	Rb	0.01	0.23
Ba	220	812	OX	0.64	0.1	Ba	0.05	0.83
Sr	330	187	PLG	0.15	0.57	Sr	0.29	2.02
Nb	9	8	KF	0	0.07	Nb	0.28	0.26
Y	16.5	21	BT	0	0.04	Y	0.35	0.52
Th	3.3	15.2	AP	0	0.01	Th	0.04	0.13
La	14.7	44	QZ	0	0.14	La	0.05	0.26

[a]Composition of the basic magma corresponding to that of the estimated CCB parental magma (Table 7).
[b]Composition of the contaminant magma corresponding to sample SP241.
[c]Average mineral fractionating assemblages calculated by MELTS.
[d]Bulk partition coefficients calculated using K_d^s given in Table 10.
Element concentrations in ppm. Rate of assimilation over fractionation (r) is 0.6 and 0.45 for CFC 1 and CFC 2, respectively.

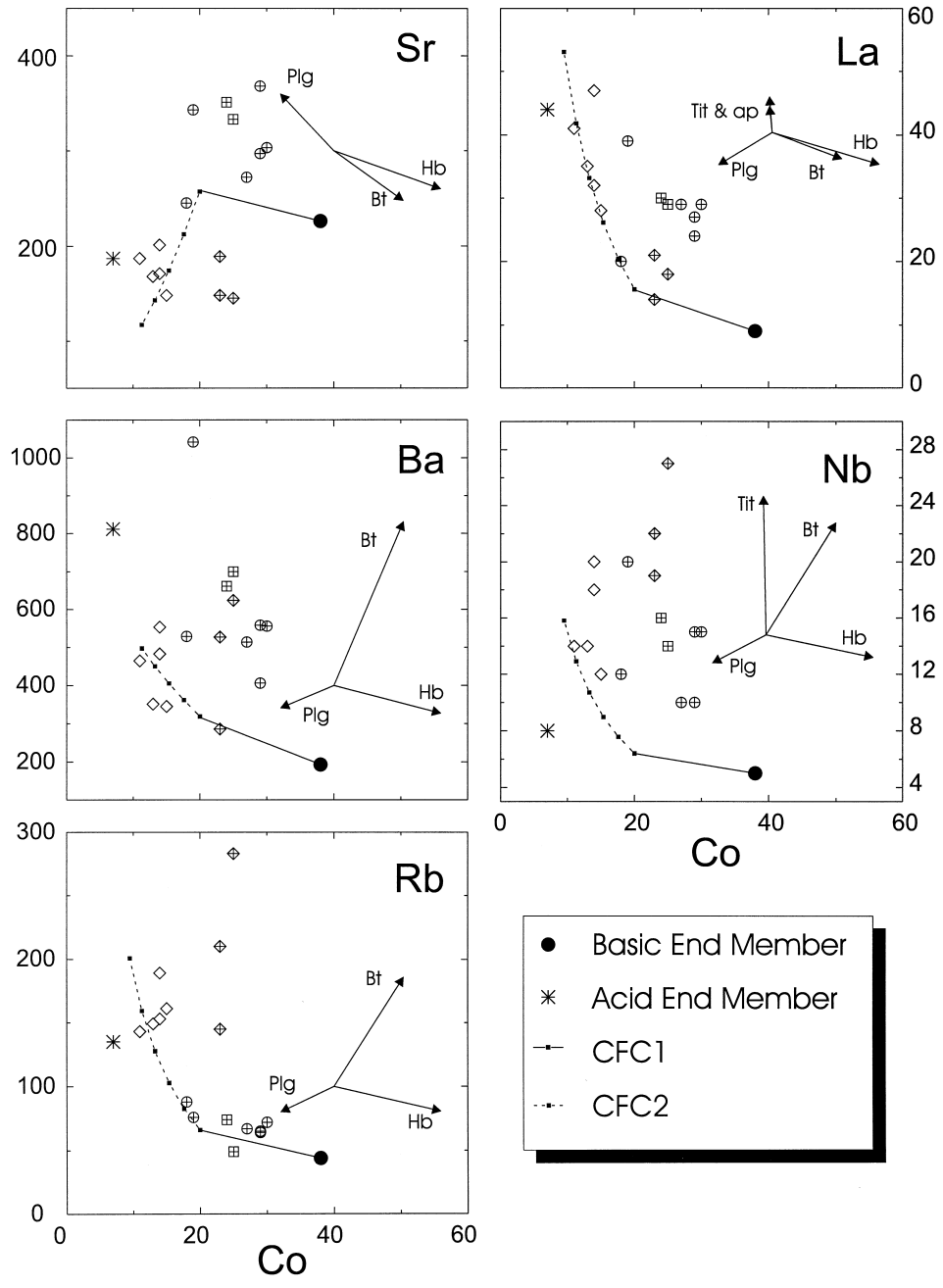

Fig. 5. Interelemental binary diagrams showing the CFC differentiation process responsible for the genesis of the mafic enclaves (MMEt and MMEg), and the outer facies of the CCB and BS. The first step (CFC1) is up to 8% of crystal fractionation. Tick marks on the second step liquid line of descent (CFC2) are reported at 10% interval of crystal fractionation. Mineral vectors indicate the direction of displacement expected for mineral accumulation corresponding to 20% (main minerals) and 1% (accessory minerals). Since thermodynamic data for amphibole are not included in MELTS (Ghiorso et al., 1994), we have used the amount of crystallising clinopyroxene as a proxy for amphibole on the basis of petrographic observation. The equation used for the CFC modelling is from DePaolo (1981). Symbols not in the legend as in Fig. 3.

Table 9
Chemical analyses of minerals used in the differentiation process of the inner facies of the Capo Carbonara basic complex (CCB_{inn})

	PLG (An_{85})	CPX	HB	OX
SiO_2	46.44	51.67	50.95	0.00
TiO_2	0.00	0.08	0.57	0.14
Al_2O_3	34.34	0.62	4.65	0.00
Fe_2O_3	0.13	1.58	2.63	68.97
FeO	–	12.39	9.31	31.25
MnO	–	1.37	0.32	0.02
MgO	–	10.49	17.19	0.00
CaO	17.21	22.07	11.43	0.00
Na_2O	1.69	0.23	0.67	0.00
K_2O	0.04	0.00	0.19	0.00
Total	99.85	100.50	97.91	100.38

due to a *filter pressing* process operating during the crystallisation and contamination of the basic magma, which squeezed out some portions of the residual liquid and determined the 'cumulitic' signature of the samples with no textural evidence (e.g., Pearce et al., 1984). As an example, we reported in Fig. 5 the displacement vectors originating from 'cumulus' of 20% and 1% of the main and accessory minerals, respectively. Although such vectors represent an oversimplification, it is clear from Fig. 5 that trace element contents can be significantly deviated from the calculated liquid line of descent in response to 'cumulus' of main and accessory minerals. In particular, the trace element variation of the outer facies of the CCB and BS is consistent with 'cumulus' of plagioclase and clinopyroxene/amphibole mainly during the first step of CFC, whilst that of the gabbro-dioritic mafic enclaves is consistent with 'cumulus' of hornblende and biotite mainly during the second step of CFC (Fig. 5). This is evident in the Rb and Sr vs. Co diagrams (Fig. 5): the outer facies of the CCB and BS have different contents of Rb and Sr with respect to the gabbro-dioritic mafic enclaves just because of the different amount of plagioclase vs. biotite among their relative 'cumulus' assemblage. Considering accessory minerals, it is clear the important role of apatite and titanite in displacing La and Nb contents of the samples from the liquid line of descent. The involvement of such minerals during the CFC modeling agrees with the petrographic features of the samples.

In summary, although the geochemistry of the gabbro-dioritic mafic enclaves and the outer facies of the CCB and BS can be explained by the same physical process, i.e., filter pressing, the amount of minerals entered the 'cumulus' assemblage has determined different geochemical signatures in the two groups of rocks. The gabbro-dioritic mafic enclaves and the outer facies of the CCB and BS could represent mixtures between the trapped residual liquid and different amounts of minerals crystallised during the interaction of the acid and basic magmas. Trace element variations are consistent with 'cumulus', via filter pressing, of the mineral assemblages calculated by MELTS with addition of a number of accessory phases (zircon, titanite) not taken into account for by MELTS. The proposed process is able to readily explain the apparent alkaline character of the gabbro-dioritic mafic enclaves (unusual for this suite of calc-alkaline rocks), due to 'cumulus' of biotite that determined an increase in K_2O and a decrease in SiO_2.

Sr and Nd isotope ratios display quite a different behaviour from trace elements. Applying the CFC process to isotopic ratios and using the same parameters as for trace elements, we are unable to reproduce the $^{87}Sr/^{86}Sr$ and $^{143}Nd/^{144}Nd$ of the mafic enclaves. There is a hint that this common behaviour of isotopes in acid–basic magma interaction products (e.g., Pin et al., 1990; Holden et al., 1991; Tom-

Table 10
Set of partition coefficients employed in the differentiation process of the inner facies of the CCB complex and in the CFC process

	CPX	HB	OX	PLG	BT	KF	AP
Co	1.5	3	6.6	0	23	0	0
Rb	0.02	0.03	0	0	5.3	0.3	0
Ba	0.03	0.09	0	0.26	6.36	6	0
Sr	0.05	0.33	0	1.7 *	0.12	3 *	2
Nb	0.03	0.2	0.4	0	5	0.1	0
Y	0.7	1.47	0.2	0	0.6	0.01	40
Th	0.01	0.1	0	0.2	0.2	0.02	0
La	0.05	0.16	0.01	0.14	0.3	0.07	15

Partition coefficients from the compilation in GERM (1997). CPX: clinopyroxene; HB: amphibole; OX: oxide; PLG: plagioclase; BT: biotite; KF: K-feldspar; AP: apatite. Partition coefficients for quartz are assumed zero.
* K_d of Sr in PL and KF are 3 and 3.8 in the second step of CFC, respectively.

masini, 1993) could be controlled by another mechanism superimposed to the CFC process, i.e., liquid-state isotope diffusion. This mechanism can, in principle, explain the decoupling of isotopes (essentially homogeneous in mafic enclaves and host granites), from trace elements (preserving significant heterogeneities in mafic enclaves and host granites), since liquid-state isotope diffusion is up to two order of magnitude more rapid than elemental diffusion (Baker, 1989; Lesher, 1994). The occurrence of liquid-state isotope diffusion has been already proposed to explain the relative uniformity of isotopic ratios in the products originating from magma interaction that outcrop in another sector of the Sardinia–Corsica Batholith (Poli et al., 1996). We cannot explore the details of this mechanism with the available isotopic data on the Sarrabus rocks, but simply suggest that this process deserves focused studies to unravel its bearing in controlling the evolution of isotopic ratios during acid–basic magma interaction.

Acknowledgements

The authors wish to thank Piero Manetti and Angelo Peccerillo for very useful discussions and suggestions, and Lorella Francalanci for her invaluable help. Research was financially supported by Italian MURST Grants 40% and Italian CNR funds to G.P.

References

Baker, D.R., 1989. Tracer versus trace element diffusion: diffusional decoupling of Sr concentration from Sr isotope composition. Geochim. Cosmochim. Acta 53, 3015–3023.

Bralia, A., Ghezzo, C., Guasparri, G., Sabatini, G., 1981. Aspetti genetici del batolite sardo-corso. Rend. Soc. Ital. Mineral. Petrol. 238, 701–764.

Campbell, I.H., Turner, J.S., 1989. Fountain in magma chambers. J. Petrol. 30, 885–923.

Carmignani, L., Barca, S., Carosi, R., Di Pisa, A., Gattiglio, M., Musumeci, G., Oggiano, G., Pertusati, P.C., 1992. Schema dell'evoluzione del Basamento Sardo. In Struttura della catena ercinica in Sardegna. Informal Group of Structural Geology, Field-book, pp. 11–38.

Cawthorn, R.G., 1996. Layered Intrusions. Elsevier, Amsterdam, 531 pp.

Cocherie, A., 1984. Interaction manteau-croute: son role dans la genese d'associations plutonuques calco-alcalines, contraines geochimiques (element en traces et isotopes du strontium et de ll'oxigen). Unpublished PhD thesis, University of Rennes, 245 pp.

Cocherie, A., Rossi, P., Fouillac, A.M., Vidal, P., 1994. Crust and mantle contributions to granite genesis—an example from the Variscan batholith of Corsica, France, studied by trace element and Nd–Sr–O-isotope systematics. Chem. Geol. 115, 173–211.

DePaolo, D.J., 1981. Trace element and isotopic effects of combined wallrock assimilation and fractional crystallization. Earth Planet. Sci. Lett. 53, 189–202.

Didier, J., Barbarin, B., 1991a. Enclaves and Granite Petrology. Elsevier, Amsterdam, p. 625.

Didier, J., Barbarin, B., 1991b. The different types of enclaves in granites. in: Didier, J., Barbarin, B. (Eds.), Enclaves and Granite Petrology. Elsevier, Amsterdam, pp. 19–23.

Franzini, M., Leoni, L., 1972. A full matrix correction in X-ray fluorescence analysis of rock samples. Atti Soc. Toscana Sci. Nat. Mem. (A) 79, 7–22.

Frost, T.P., Lindsay, J.R., 1988. Magmix: a basic program to calculate viscosities of interacting magmas of differing composition, temperature, and water content. Computers and Geosciences 14, 213–228.

Ghiorso, M.S., Hirschmann, M., Sack, R.O., 1994. MELTS: software for thermodynamic modeling of magmatic systems. EOS 75, 571.

Haskin, L.A., Frey, L.A., Schmitt, R.A., Smith, R.H., 1966. Meteoric, solar and terrestrial abundances of the rare earth. Phys. Chem. Earth 7, 167–321.

Henderson, P., 1986. Inorganic Geochemistry. Pergamon, Oxford, 353 pp.

Holden, P., Halliday, A.N., Stephens, W.E., Henney, P.J., 1991. Chemical and isotopic evidence for major mass transfer between mafic enclaves and felsic magma. Chem. Geol. 92, 135–152.

Irvine, T.N., 1979. Rocks whose composition is determined by crystal accumulation and sorting. in: Yoder, Y. (Ed.), The Evolution of Igneous Rocks. Princeton University Press, Princeton, pp. 245–306.

Irvine, T.N., 1980. Magmatic infiltration metasomatism, double diffusive fractional crystallization, and adcumulus growth in the Muskox intrusion and other layered intrusions. in: Hargraves, L. (Ed.), Physics of Magmatic Processes. Princeton University Press, Princeton, pp. 325–384.

Kaye, M.J., 1965. X-ray fluorescence determinations of several trace elements in some standard geochemical samples. Geochim. Cosmochim. Acta 29, 139–142.

Lesher, C.E., 1994. Kinetics of Sr and Nd exchange in silicate liquids: theory, experiments, and applications to uphill diffusion, isotopic equilibration, and irreversible mixing of magmas. J. Geophys. Res. B 5 (99), 9585–9604.

Nakajima, Y., Ribbe, P.H., 1981. Texture and structural interpretation of the alteration of pyroxene to other biopyroboles. Contrib. Mineral. Petrol. 78, 230–239.

Nicoletti, M., Ardanese, L.R., Colasanti, S., 1982. La granodiorite di Capo Carbonara (Sardegna, Italy). Età K/Ar di fasi minerali in paragneiss. Rend. Soc. Ital. Mineral. Petrol. 38, 765–769.

Pearce, J.A., Harris, N.B., Tindle, A.G., 1984. Trace element discrimination diagrams for the tectonic interpretation of granitic rocks. J. Petrol. 25, 956–983.

Pin, C., Binon, M., Belin, J.M., Barbarin, B., Clemens, J.D., 1990. Origin of microgranular enclaves in granitoids: equivocal Sr Nd isotopic evidence from Hercynian rocks in the Massif Central (France). J. Geophys. Res. 95, 17821–17828.

Poli, G., Tommasini, S., 1991. Model for the origin and significance of microgranular enclaves in calc-alkaline granitoids. J. Petrol. 32, 657–666.

Poli, G., Manetti, P., Peccerillo, A., Cecchi, A., 1977. Determinazione di alcuni elementi del gruppo delle terre rare in rocce silicatiche per attivazione neutronica. Rend. Soc. Ital. Mineral. Petrol. 33, 755–763.

Poli, G., Ghezzo, C., Conticelli, S., 1989. Geochemistry of granitic rocks from the Hercynian Sardinia–Corsica Batholith: implication for magma genesis. Lithos 23, 247–266.

Poli, G., Tommasini, S., Halliday, A.N., 1996. Trace element and isotopic exchange during acid–basic magma interaction processes. Trans. R. Soc. Edinb. 87, 225–232.

Rossi, P., Cocherie, A., 1991. Genesis of a Variscan batholith: field, petrological and mineralogical evidence from the Corsica–Sardinia Batholith. Tectonophysics 195, 319–346.

Tommasini, S., 1993. Petrologia del Magmatismo Calcalcalino del Batolite Sardo-Corso: processi genetici ed evolutivi dei magmi in aree di collisione continentale e implicazioni geodinamiche. Unpublished PhD thesis, University of Perugia, 326 pp.

Tommasini, S., Poli, G., 1992. Petrology of the late-Carboniferous Punta Falcone gabbroic complex, northern Sardinia, Italy. Contrib. Mineral. Petrol. 110, 16–32.

Tommasini, S., Poli, G., Halliday, A.N., 1995. The role of sediment subduction and crustal growth in Hercynian plutonism: isotopic and trace element evidence from the Sardinia–Corsica Batholith. J. Petrol. 36, 1305–1332.

Vernon, R.H., 1984. Microgranitoid enclaves in granites—globules of hybrid magmas quenched in a plutonic environment. Nature 309, 438–439.

Wager, L.R., Brown, G.M., 1967. Layered Igneous Rocks. Freeman, San Francisco.

Wilson, M., 1989. Igneous Petrogenesis. Unwin Hyman, London, 466 pp.

Wright, T.L., Doherty, P.C., 1970. A linear programming and least squares computer method for solving petrologic mixing problems. Geol. Soc. Am. Bull. 81, 1995–2008.

Zorpi, M.J., Coulon, C., Orsini, J.B., 1991. Hybridization between felsic and mafic magmas in calc-alkaline granitoids—a case study in northern Sardinia, Italy. Chem. Geol. 92, 45–86.